Macromolecules

ARTICLE

pubs.acs.org/Macromolecules

Domain Orientation and Grain Coarsening in Cylinder-Forming Poly(styrene-*b*-methyl methacrylate) Films

Shengxiang Ji,[†,‡] Chi-Chun Liu,[†] Wen Liao,[†] Alyssa L. Fenske,[†] Gordon S. W. Craig,[†] and Paul F. Nealey*[,†]

[†]Department of Chemical and Biological Engineering, University of Wisconsin, 1415 Engineering Drive, Madison, Wisconsin 53706, United States

[‡]Key Laboratory of Polymer Ecomaterials, Changchun Institute of Applied Chemistry, Chinese Academy of Sciences, Changchun 130022, China

Supporting Information

ABSTRACT: The domain orientation and grain sizes in cylinder-forming poly(styrene-*b*-methyl methacrylate) (PS-*b*-PMMA) films were systematically investigated as a function of film thickness (32−640 nm), annealing temperature (190−230 °C), and wetting behavior of PS-*b*-PMMA on substrates. The domain orientation at the film surface depended on film thickness as well as both the polymer−substrate and polymer−free surface boundary conditions. In thin films (thickness $L < 3L_0$, where L_0 is the domain period of the block copolymer), the polymer−substrate boundary condition dominated and determined the domain orientation of the block copolymer. At intermediate thicknesses ($3L_0 < L < 6L_0$) the interplay of both boundary conditions usually resulted in the formation of a mixed structure. In films with $L > 6L_0$, the two boundary conditions decoupled, and the polymer-free surface interaction determined the domain orientation of cylinders near the film surface regardless of the chemistry of the underlying substrate. The orientational correlation length (ξ) of grains of perpendicular cylinders at the surface increased with the increase of annealing temperature for films of equal L. The grains coarsened at 210 and 230 °C, and the corresponding ξ's scaled with annealing time (t) according to a power law, $\xi \sim t^{\phi}$, with $\phi = 0.28 \pm 0.01$. ξ's also increased linearly with L. In films annealed at 190 °C, the ξ's were nearly constant with increasing L. The technical significance of this work is that the surface domain pattern with a large ξ can be achieved on the surface of thick films and the surface pattern can be successfully replicated by molecular transfer printing (MTP) to create a chemical pattern with the same ξ without the use of lithographic tools.

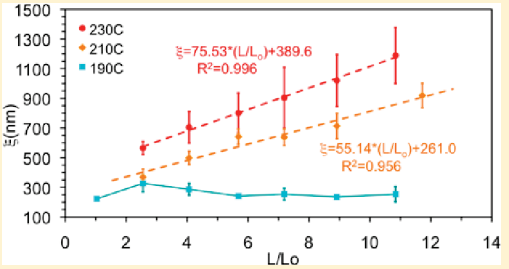

INTRODUCTION

Block copolymers can spontaneously phase separate into well-ordered, periodic structures with dimensions in the range 5−50 nm.[1] In thin films, block copolymers usually have a much richer range of morphologies than in bulk due to the boundary conditions at both the substrate and free surface.[2−14] The interplay between the polymer−substrate interaction and the polymer−free surface interaction can also determine the domain orientation in films. Strongly preferential wetting of one block to the substrate usually leads to the formation of a parallel orientation of lamellar or cylindrical domains.[15−17] A perpendicular orientation of block copolymer domains can be obtained near the substrate region through careful control of the substrate chemistry by using self-assembled monolayers,[18−20] random copolymer brushes,[21−25] binary homopolymer blend brushes,[16] block cooligomer brushes,[26] or chemical nanopatterning.[9−13,27−31] The perpendicular domains may propagate through the entire film thickness if the surface energy (γ) of both blocks of the block copolymer are nearly equal, which can be the case with poly(styrene-*b*-methyl methacrylate) (PS-*b*-PMMA) at certain combinations of molecular weight (M_n) and annealing temperature (T).[23,32] For most block copolymers, the γ values of the two blocks are sufficiently different to lead to the formation of a parallel orientation of domains or a wetting layer at the free surface, regardless of the substrate chemistry and the domain orientation near the substrates.[33−35] Even with PS-*b*-PMMA, the dependence of γ on T and M_n can cause the γ values of the PS and PMMA blocks to be sufficiently different, leading to parallel domains at the free surface of a PS-*b*-PMMA film.[17,36,37]

A number of studies have been performed to examine the domain orientation in relatively thicker films of PS-*b*-PMMA as a function of the film thickness, L, and the interfacial energy between the substrate and PS and PMMA blocks. Xu et al. studied the domain orientation of lamellar-forming PS-*b*-PMMA on both preferential and nonpreferential substrates by cross-sectional transmission electron microscopy.[17] On nonpreferential substrates, they observed a mixed structure with perpendicular lamellae near the substrate region and parallel lamellae at the free surfaces. When the PS-*b*-PMMA film was on a preferential substrate, a more complex 3-dimensional structure formed,

Received: March 13, 2011
Revised: April 12, 2011
Published: April 29, 2011

with parallel lamellae near both interfaces and perpendicular lamellae in the middle. In a study of PS-*b*-PMMA films on silicon substrates, Zhang et al. observed the transition from parallel cylinders to a mixture of parallel and perpendicular cylinders on the surfaces of films as L was increased beyond ~3−4 times the bulk row-to-row period, L_0.[38] Suh et al. studied the effect of L on the domain orientation in lamellae-forming PS-*b*-PMMA films on organosilicate substrates with non-preferential and weakly preferential wetting for PS and PMMA and observed and modeled the oscillation between perpendicular and parallel lamellar domains with the increase of L.[39]

Along with the orientation of block copolymer domains, it is also important to understand the ordering of the domains. Self-assembly of block copolymers typically results in the formation of grains that can coarsen upon annealing. Efforts have been made to quantify the size and growth of grains of domains of block copolymers in thin films.[15,30,40−43] Harrison et al. first studied the time evolution of stripe patterns of cylindrical copolymers in thin films and found that the correlation length (ξ) scaled with the annealing time (t) according to a power law, $\xi \sim t^{\phi}$, where $\phi = 0.25$.[15,42] Harrison et al.[41] and Vega et al.[43] also measured the ξ's of spot patterns from sphere-forming block copolymers in thin films. The spot patterns also coarsened according to a power low ($\phi \approx 0.25$), but with a different coarsening mechanism. In a closely related study, Black et al. investigated the ordering kinetics of perpendicular cylinders in films with $L = L_0$, and the grain growth followed the same power law ($\phi \approx 0.25$).[40] For perpendicular lamellae, ξ did not change noticeably with annealing time when $L = L_0$, but scaled as $\xi \sim t^{0.11}$ when $L = 0.5L_0$.[30] In all cases, the ordering kinetics in thin films was much slower than that in bulk ($\phi \approx 1.05$).[44]

The surface domain pattern with long-range order is desirable for a number of applications. Solvent annealing,[45] graphoepitaxy,[6] and chemical nanopatterning[9] have been widely studied to achieve nanostructures with long-range order. Recently, Ji et al. developed an approach to preparing arrays of perpendicularly oriented PS-*b*-PMMA cylinders with long-range orientational order at the film surface on silicon substrates by a combination of high annealing T and large L.[46] At such high annealing T (~210−230 °C), γ of PS and PMMA appeared to be nearly equal,[23] leading to the formation of perpendicular cylinders at the free surface. The use of thick films eliminated any effect the substrate could have had on the domain orientation near the film surface region. In a related study, Han et al. reported the formation of perpendicularly oriented cylinders on neutral surfaces in films with L up to 900 nm.[32] In thicker films, however, separate cylinder formation events simultaneously occurred at the substrate interface and the free surface, and the cylinders from each surface propagated toward the middle of the film. As a result, two propagation fronts merged within the film, and it is likely that while the domains were perpendicular to the substrate, they were not continuous throughout the film. To make better use of such large grains on film surfaces, a pattern transfer strategy is needed; however, the noncontinuity of domains in the thick film makes it difficult to pattern transfer into the underlying substrate. Instead of pattern transfer through the entire film thickness, molecular transfer printing (MTP) could be used to replicate the domain pattern present at the film surface to create a chemical pattern.[46] The replica chemical pattern could direct the assembly of a thin film, a superior template for pattern transfer, of the same block copolymer.

In the work presented here, we systematically studied the evolution of surface morphologies in cylinder-forming PS-*b*-PMMA films as a function of the annealing temperature, film thickness, and substrate chemistry. We also quantified the grain coarsening of the polycrystalline grains of perpendicular cylinders with respect to the annealing temperature, film thickness, and substrate chemistry. Finally, we demonstrated that we could fabricate hexagonal chemical patterns with large desirable ξ without requiring advanced lithography tools by replicating the surface domain patterns of thick films by MTP. The chemical pattern was subsequently used to direct the assembly of a thin film of block copolymer for pattern transfer into the underlying substrate.

EXPERIMENTAL SECTION

Materials. Cylinder-forming PS-*b*-PMMA (**C4621**, M_n = 46−21 kg/mol, L_0 = 31.5 nm (row-to-row), PDI = 1.06), hydroxyl-terminated polystyrene (PS-OH, M_n = 6 kg/mol, PDI = 1.05), and hydroxyl-terminated poly(methyl methacrylate) (PMMA-OH, M_n = 6 kg/mol, PDI = 1.05) were purchased from Polymer Source, Inc., and used as received. Hydroxyl-terminated random copolymer poly(styrene-*r*-methyl methacrylate) (PS-*r*-PMMA-OH) was synthesized by nitroxide-mediated radical polymerization[47] to contain 63 wt % styrene fraction (denoted as **63S**), with M_n = 9.6 kg/mol and PDI = 1.20, as determined by ^{1}H nuclear magnetic resonance spectroscopy.

Sample Preparation. Silicon wafers were cleaned by oxygen plasma treatment on a PE-200 Benchtop Plasma System (Plasma Etch, Inc.) prior to use. PS-*r*-PMMA-modified substrates were prepared by spin-coating a 1 wt % solution of **63S** in toluene at 4000 rpm on silicon substrates, followed by annealing at 160 °C for 48 h under vacuum. Ungrafted **63S** was removed by repeated sonication in warm toluene. C4621 films with L ranging from 32 nm (~1L_0) to 630 nm (~20L_0), as determined by a Rudolph ellipsometer and a Filmetrics reflectometer, were deposited from toluene solutions with concentrations of 1−9 wt % on bare silicon and **63S**-modified silicon substrates. Samples were annealed at 190, 210, or 230 °C for times (0.5 min−24 h) under vacuum or a nitrogen atmosphere.

Image Analysis. After thermal annealing, block copolymer films were etched for 10 s in a Uniaxis 790 reactive ion etcher (Plasma-Therm, Inc.) at 35 °C, 50 W power, 10 mTorr pressure, and an oxygen flow rate of 10 sccm to remove the PMMA block near film surfaces. The etch rates were ~40 nm/min for PS and ~95 nm/min for PMMA. Samples were then sputtered with a thin layer (~1 nm) of Au to facilitate imaging by scanning electron microscopy (SEM, LEO 1550 VP field-emission SEM with 1 kV accelerating voltage). Five SEM images were taken from different areas on each sample. The size of each image was 4.2 μm × 5.6 μm. The images were processed using a Matlab program which performed four operations on each image: image binarization, domain centroid localization, defect exclusion, and calculation of the autocorrelation function (ACF).[48] The centers of PMMA domains in SEM images are located through a set of "standard" image processing routines. Since the background intensity and the image quality in our SEM images are usually uniform, a simple thresholding technique was used to convert the grayscale image to a binary image. The Otsu's method was then employed to minimize the intraclass variance of the foreground and background pixels and automatically select the threshold value.[49] A Matlab built-in function was then used to convert the pixels brighter than the threshold to "white pixels" and the pixels darker than the threshold to "black pixels". The orientational correlation length ξ of the perpendicular cylinders was calculated by fitting the

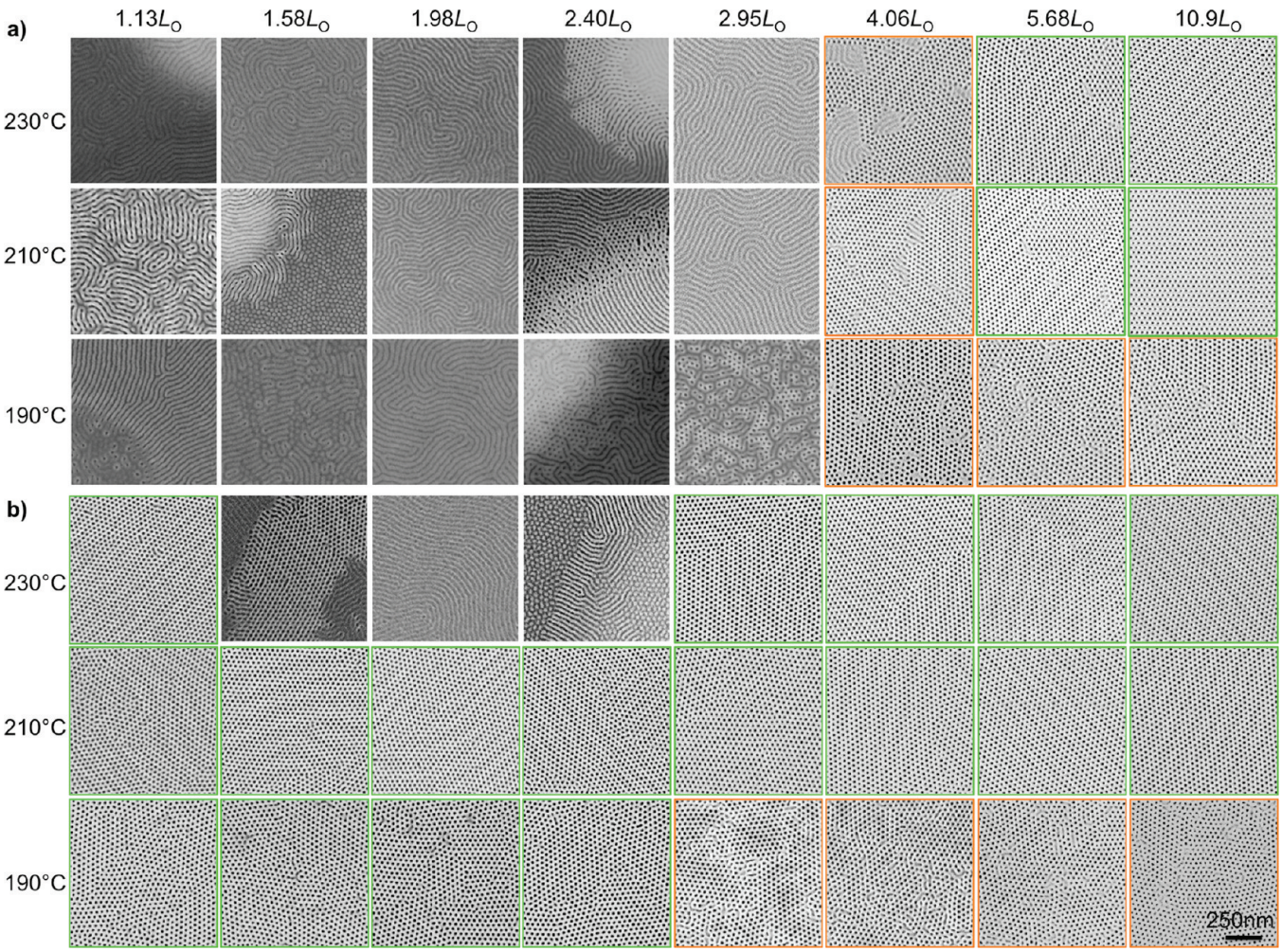

Figure 1. Top-down SEM images of C4621 films with various thicknesses ($1.13L_0-10.9L_0$) annealed at different temperatures (230, 210, and 190 °C) for 24 h on (a) silicon substrates and (b) **63S**-modified silicon substrates. Green, brown, and red colors indicate defect-free perpendicular cylinders, nearly defect-free perpendicular cylinders with few parallel cylinders, and perpendicular cylinders with large grains of parallel cylinders, respectively. The rest of the images show either parallel cylinders or island structures, as seen in the change of brightness or morphology.

ACF to an exponential function using

$$\mathrm{ACF} = \exp\left(-\frac{r}{\xi}\right) \quad (1)$$

where r is the distance from the center domain in the ACF analysis.

Molecular Transfer Printing (MTP) and Pattern Transfer. The MTP process was demonstrated and detailed in the paper by Ji et al.[46] A schematic of the MTP process is shown in Figure 7a. A 300 nm thick ternary blend film containing 90 wt % C4621, 7 wt % PS-OH, and 3 wt % PMMA-OH was deposited on a **63S**-modified substrate and annealed at 230 °C for 24 h. PS-OH and PMMA-OH served as inks and were segregated into their respective PS and PMMA domains in PS-*b*-PMMA block copolymers upon annealing. We intentionally chose a 300 nm thick ternary blend film as the master film since huge grains of perpendicular cylinders could be obtained on the surface in films with $L > 200$ nm (or $6L_0$) under 230 °C annealing. A 30 nm thick silicon oxide layer was evaporated onto the surfaces of the ternary blend film using a Telemark eBeam evaporator. An oxygen-plasma-cleaned silicon substrate was placed in contact with the oxide surface. The sandwiched structure was clamped by a parallel four-screw clamp and annealed at 160 °C for 24 h under vacuum. Upon annealing, PS-OH and PMMA-OH reacted with the silanol groups on the surface of the replica substrate through a dehydration reaction, replicating the domain pattern present at the surface of the master film. The sandwiched structure was then separated by dissolving block copolymers and unreacted homopolymers by repeated sonication in chlorobenzene to create a replica chemical pattern.[46] The replica was then used to direct the assembly of a 30 nm thick C4621 film that was annealed at 190 °C for 24 h. The PMMA domains were removed by UV exposure (XL-1500 UV cross-linker, Spectronics Corp., λ = 254 nm, dose = 350 mJ/cm^2) and acetic acid washing (1 min). The brush layer was etched by an oxygen plasma in a Unaxis 790 reactive ion etcher. Pattern transfer into the underlying silicon oxide layer was performed using a $C_2H_2F_4/SF_6$ plasma in a Helicon high-density plasma tool.[50]

RESULTS

The effect of the substrate and free surface on the domain orientation in C4621 films of various L ($\sim 1L_0-11L_0$) annealed at different T (190−230 °C) for 24 h can be observed in the top-down SEM images presented in Figure 1. Two different substrates were used: an untreated silicon substrate with a layer of native oxide which is preferentially wet by the PMMA block and a

dx.doi.org/10.1021/ma2005734 |*Macromolecules* 2011, 44, 4291–4300

silicon substrate coated with **63S** which is in the nonpreferential composition range for cylinder-forming PS-*b*-PMMAs. The effect of free surface on the surface domain orientation could be effectively modulated by the annealing temperature. At 190 °C, PS has a slightly lower γ than PMMA[37] and prefers to reside at the free surface of the film, while the γ values for PS and PMMA are nearly equal at 210−230 °C and the free surface is nonpreferential surface to both blocks in PS-*b*-PMMA.[51]

Figure 1a shows SEM images of C4621 films that were annealed at 190−230 °C on silicon substrates. In general, the surface morphology progressed from parallel cylinders in thinner films ($L < 2.95L_0$) to perpendicular cylinders in thicker films ($L > 4.06L_0$) that were annealed at 230 °C. A complex morphology transition happened in films with $L < 2.95L_0$. Islands (seen as regions of markedly different brightness in the SEMs) formed with initial thicknesses of $\sim 1.13L_0$ and $2.40L_0$, but the final thicknesses were quantized with L of $\sim 2L_0$ and $3L_0$ on top of the islands, respectively. The structures on islands were similar to the parallel cylinders on films with initial thicknesses of $1.98L_0$ and $2.95L_0$ at which cylinders were parallel to the surface. Perforated structures which were dissimilar to the parallel cylinders in the film with $L = 1.98L_0$ formed in the film with $L = 1.58L_0$ and the film was flat. For films where $3L_0 < L < 6L_0$, e.g., $L = 4.06L_0$ and $5.68L_0$, a mixture of parallel and perpendicular cylinders formed at film surfaces and the percentage of perpendicularly orientated cylinders increased with the increase of L. The island (or hole) formation was also suppressed even when L is not quantized. As L was increased beyond $5.68L_0$, larger L and higher annealing T both led to improved hexagonal order of perpendicular cylinders on the film surface, as shown in the representative film with $L = 10.9L_0$. The morphologies of C4621 films on untreated silicon substrates annealed at 210 °C were different from those at 230 °C in films with $L = 1.13L_0$ and $1.58L_0$ and the same as those at 230 °C in films with $L > 1.98L_0$. Perforated structures formed in the film at $L = 1.13L_0$ while islands formed in the film at $L = 1.58L_0$ with a parallel cylinders on top of islands and perforated structures at the lower regions.

The morphologies observed in a third set of C4621 films on untreated silicon substrates annealed at 190 °C in Figure 1a followed the same general trend with L that was observed in the films annealed at 210 and 230 °C. As L was increased, the surface morphology transitioned from islands ($1.13L_0$) to perforated structures ($1.58L_0$) to parallel cylinders ($1.98L_0$) to islands ($2.40L_0$) to mixed parallel and perpendicular cylinders ($2.95L_0$). In addition to the improved order at $T = 210$ and 230 °C in the thickest films, there were a few noticeable differences between the films annealed at 190 °C and those annealed at 210 and 230 °C. First, the island structure observed in the film with $L = 1.13L_0$ annealed at 190 °C was similar to the perforated structure in the film with $L = 1.58L_0$ instead of that in the film with $L = 1.98L_0$ annealed at 210 and 230 °C. Second, the islands in the film with $L = 2.40L_0$ had a mixture of perpendicular and parallel cylinders, unlike the parallel cylinders observed in the same thickness film annealed at 210 and 230 °C. In addition, when $L > 2.95L_0$, parallel (or maybe capped perpendicular cylinders) and perpendicular cylinders coexisted on the film surfaces in the samples annealed at 190 °C. The fraction of parallel cylinders decreased with film thicknesses and stayed nearly constant when $L > 5.68L_0$.

The domain structures at C4621 film surfaces on **63S**-modified silicon substrates were different from those on silicon substrates

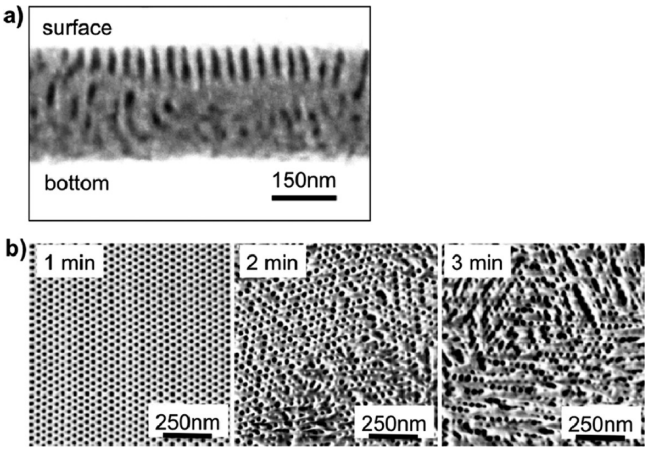

Figure 2. (a) Cross-section SEM image of a 300 nm thick C4621 film on the silicon substrate. (b) Top-down SEM images of the 300 nm thick C4621 film after different oxygen plasma etching times (1−3 min). The perpendicular cylinders preserved after 1 min etching, and the structures in 2 and 3 min etching might be due to the tilting of cylinder domains.

in films thinner than $5.68L_0$, but there was no difference in the surface structure on both substrates when the film was thicker than $5.68L_0$. On the **63S**-modified silicon substrates, a perpendicular orientation of hexagonal cylinders formed in the film with $L = 1.13L_0$ at 230 °C (Figure 1b). With increasing L, the surface morphologies transitioned from islands ($1.58L_0$) to parallel cylinders ($1.98L_0$) and then to perforated island structures ($2.40L_0$). At $L = 1.58L_0$, parallel cylinders formed on low regions while perpendicular cylinders formed on islands in the film. At $L = 2.40L_0$, parallel cylinders formed at the transition regions with perforated structures at both high and low regions in the film. When the film was thicker than $2.95L_0$, the formation of perpendicular cylinders was always observed. Two sets of C4621 films on **63S**-modified silicon substrates were also annealed at 210 and 190 °C (Figure 1b). A perpendicular orientation of cylinders formed at surfaces in films annealed at 210 °C regardless of the film thickness. For films annealed at 190 °C, perpendicular cylinders formed in films with $L < 2.40L_0$. A mix of perpendicular and parallel cylinders (or looping structures) was observed on film surfaces when $L > 2.95L_0$. The percentage of parallel cylinders decreased with the increase of L and stayed nearly constant when $L > 5.68L_0$.

The domain orientation within a film on the silicon substrate was revealed by both the top-down SEM analysis of the films after progressive oxygen plasma etching steps and cross-sectional SEM analysis.[46] The film thickness that we used was 300 nm ($9.52L_0$). At such thickness the substrate and surface effect decoupled. The films was annealed at 230 °C for 24 h. The perpendicularly oriented cylinders did not propagate through the entire film thickness from the top-down SEM analysis of the etched samples (Figure 2b). The fact that the cylinders did not propagate through the entire film thickness was also evidenced in SEM images of films after progress removal of top layers. After 1 min of etching the perpendicular cylinders were still well-ordered, but after 2 min of etching, a number of defect structures appeared that could have been caused by tilted cylinders. The number of such defect structures increased as the etch was continued for another 1 min. These results agreed with the cross-sectional SEM image (Figure 2a), in which

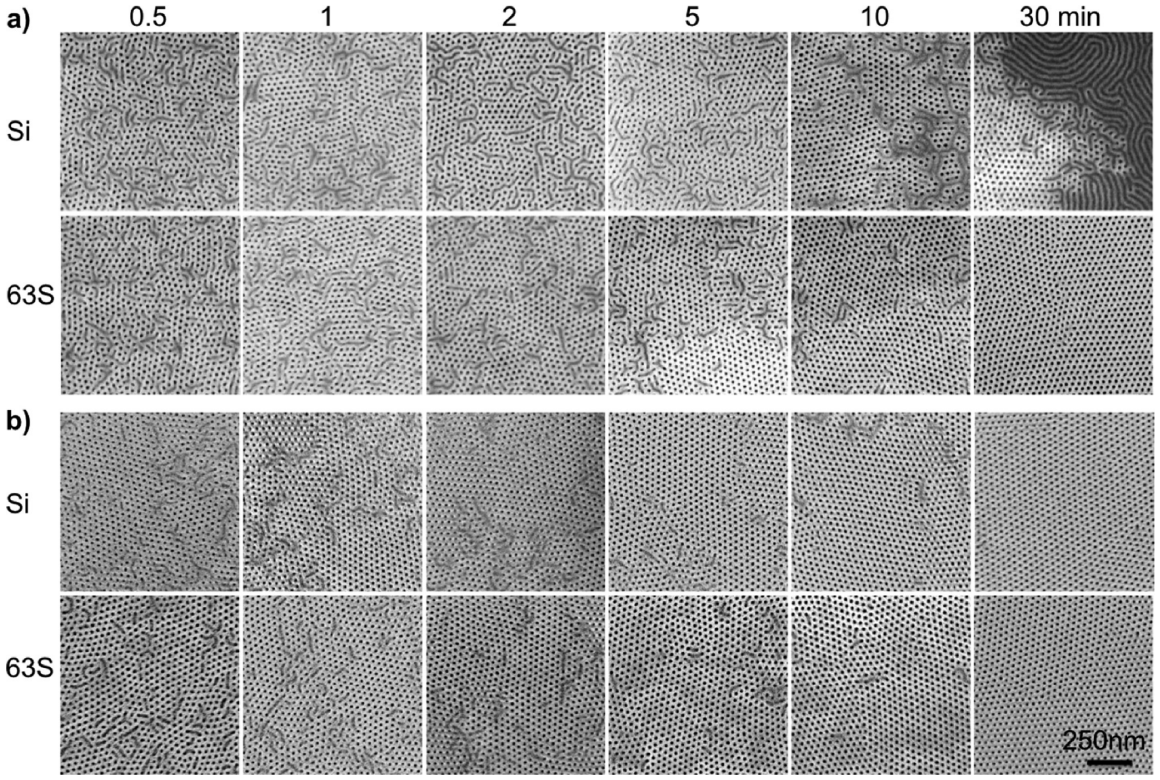

Figure 3. Assembly dynamics of (a) 95 nm thick ($3.02L_0$) and (b) 340 nm thick ($\sim 10.8L_0$) C4621 films on silicon and **63S**-modified substrates at 230 °C. Samples were annealed for 0.5−30 min under a nitrogen atmosphere.

approximately 2−3 layers of parallel cylinders were observed near the silicon substrates.

All of samples shown in Figures 1 and 2 were annealed for 24 h. To probe the assembly dynamics of the surface morphology of the C4621 films, the surface of the films on both silicon and **63S**-modified silicon substrates were imaged after annealing at 230 °C for times ranging from 0.5 to 30 min (Figure 3). Figure 3a shows the SEM images of the surface of 95 nm thick ($\sim 3.02L_0$) films. Phase separation occurred within 0.5 min of annealing and both parallel and perpendicular cylinders coexisted on film surfaces that were annealed for 0.5−5 min. The percentage of perpendicular cylinders increased with annealing time over the first 5 min. There was no obvious difference in morphologies between the substrates in the first 5 min of annealing. For samples annealed for 10 min, there were fewer parallel cylinders on the **63S**-modified silicon substrate than on the silicon substrate. After 30 min of annealing, the parallel cylinders completely disappeared in the film on the **63S**-modified silicon substrate, while both parallel and perpendicular cylinders coexisted and huge grains of parallel cylinders formed on the film surface on the silicon substrate. Two sets of 340 nm thick films ($10.8L_0$) on silicon and **63S**-modified silicon substrates were also compared (Figure 3b). The percentage of perpendicular cylinders increased with the annealing time and the parallel cylinders completely disappeared after 30 min annealing on both substrates. For the thick films annealed for 30 min, there was no obvious difference between the SEM images of the films on the untreated silicon substrate and on the **63S**-modified silicon substrate.

Close inspection of the top-down SEM images revealed that some of the grains were up to 2−5 μm in diameter, or as large as 10−20 μm^2 in area, in thick films that were annealed at 210 and 230 °C. The hexagonal arrays of cylinders had different grain orientations at the surface of the films, with defects that were identified as pairs of pentagons and heptagons and coded in blue and red, respectively, in the Voronoi plot shown in Figure 4a. Both isolated and conjugated pairs of pentagons and heptagons were observed, and the conjugated defects formed the grain boundaries. To better understand the effect of film thickness and annealing temperature on the grain sizes, two large SEM images (4.2 μm × 5.6 μm) that were from a 300 nm thick film annealed at 230 °C and a 50 nm thick film annealed at 190 °C for 24 h and their respective Voronoi plots are compared in Figures S1−S4. The Voronoi plots showed that these two images apparently had different grain sizes. To quantify the grain size of films, ξ was calculated with eq 1. A representative fitting of ACF is shown in Figure 4b.

The ξ's of C4621 films on both silicon and **63S**-modified silicon substrates that were annealed at 230 °C for 1.5 h are summarized in Figure 5a. 1.5 h was enough for the substrate effect to propagate through the film with $L < 6L_0$. ξ increased linearly with the film thickness up to at least $20L_0$ for films on **63S**-modified substrates. For films with thickness of $20L_0$ or more, the standard deviation of the calculated ξ was large due to the large grains and limited image size of the SEMs. As a result, we could not conclude that ξ continued to follow the linear trend at large L. Perpendicular cylinders with large grain sizes were also obtained on silicon substrates in films with $L > 6L_0$. ξ's (at 230 °C for 1.5 h) on silicon substrates also had a linear thickness dependence but were slightly smaller than those on **63S**-modified substrates of same thicknesses.

The annealing temperature also affected the grain sizes. Figure 5b shows the ξ's of three sets of C4621 films on

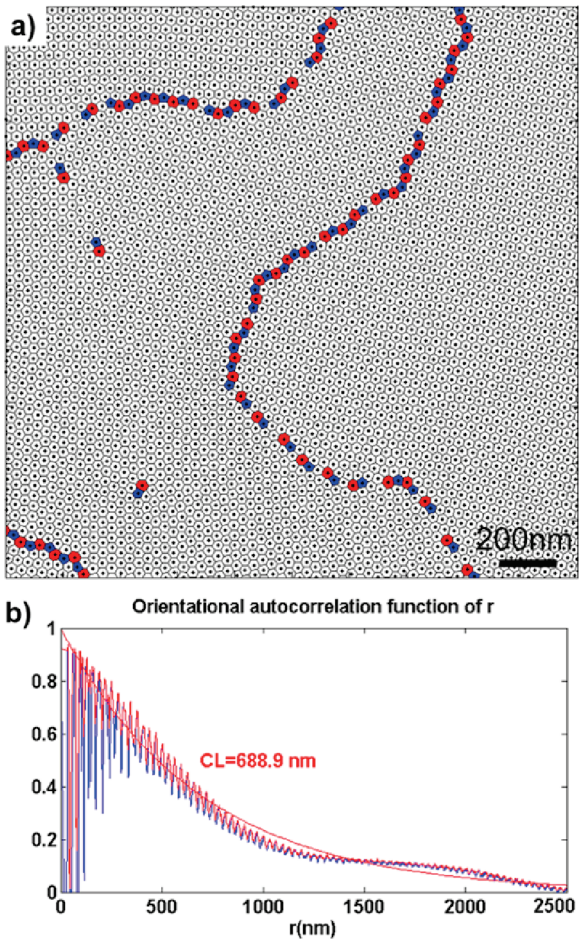

Figure 4. (a) Voronoi plot of a representative SEM image of a 300 nm thick C4621 film annealed at 230 °C for 6 h on a 63S-modified silicon substrate. Pairs of pentagons (blue) and heptagons (red) are identified as defects and conjugated defects form the grain boundary. (b) Exponential fitting of the ACF of the perpendicular cylinders in the 300 nm thick C4621 film. ξ was calculated to be ~689 nm.

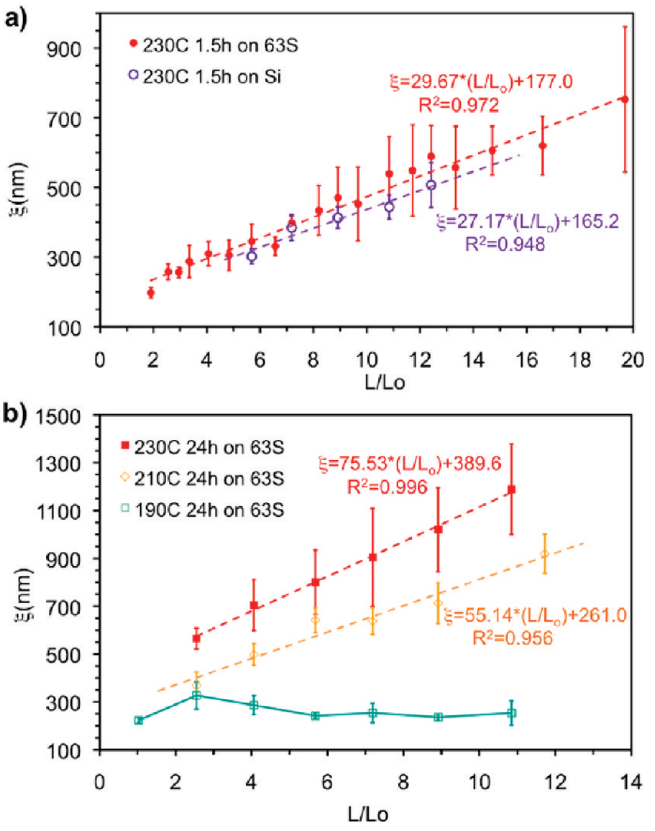

Figure 5. (a) Orientational correlation length (ξ) of perpendicular cylinders vs the thickness (L/L_0) of C4621 films on silicon (solid circles) and 63S-modified silicon (open circles) substrates at 230 °C for 1.5 h. (b) ξ vs the normalized film thickness (L/L_0) on 63S-modified silicon substrates at 230 °C (solid square), 210 °C (open diamond), and 190 °C (open square) for 24 h.

63S-modified substrates that were annealed at 230, 210, and 190 °C for 24 h. ξ increased linearly with the film thickness at 210 and 230 °C. For samples annealed at 190 °C, however, ξ was almost constant across the thickness range that we studied.

The time evolution of ξ for C4621 films on **63S**-modified substrates was also investigated, with L ranging from $2L_0$ to $11L_0$. The samples were annealed at 230 °C for 1.5, 3, 6, 12, and 24 h. As can be seen in Figure 6a, ξ once again increased linearly with L at different t (1.5−12 h). The relationship between ξ and t at different L are plotted in Figure 6b. ξ scaled with annealing time t as $\xi \sim t^{\phi}$ with $\phi = 0.28 \pm 0.01$ for the six thicknesses that were studied, which is also consistent with the cylinder- and sphere-forming systems.[15,30,40−43]

DISCUSSION

Effect of Surfaces and Film Thickness on Surface Morphology. The morphology on the surface of C4621 films can be understood in terms of the competition between the effects of the substrate interface and the free surface, which are mediated by the thickness of the film. The best example of the competition of these two effects can be seen in the SEM images of the films annealed at 210−230 °C on untreated silicon substrates. The untreated silicon prefers to be wet by PMMA, leading to the formation of parallel cylinders. At ~210−230 °C, γ for PS and PMMA are nearly equal,[23] such that the free surface functions as a neutral surface for PS and PMMA, providing the thermodynamic driving force for the formation of perpendicularly orientated cylinders. For films thinner than $3L_0$, the substrate−polymer interaction was dominant, usually leading to the formation of parallel cylinders. At the intermediate thickness range ($3L_0 < L < 6L_0$), neither the substrate interface nor the free surface dominated, resulting in the formation of both parallel and perpendicular cylinders on the film surfaces. When $L > 6L_0$, both the smoothness of the film as well as the well-ordered, perpendicular cylinders at the surface provided evidence that the polymer−surface interaction was dominant at the free surface. It appeared that perpendicular cylinders nucleated at the free surface, and then propagated from the surface toward the substrate, as seen in Figure 2a. Similar interface-dependent nucleation events were observed in the assembly of lamellar-forming PS-*b*-PMMA[17] and poly(styrene-*b*-2-vinylpyridine) (PS-*b*-P2VP).[34]

In addition to the competition between the effects of the substrate interface and the free surface, islands formed in the films with L between $1.13L_0$ and $2.40L_0$ for films annealed on untreated silicon substrates. In these films, parallel half-cylinders formed on the film surfaces in regions of the film where the local film thickness was approximately equal to nL_0, where n is an integer.

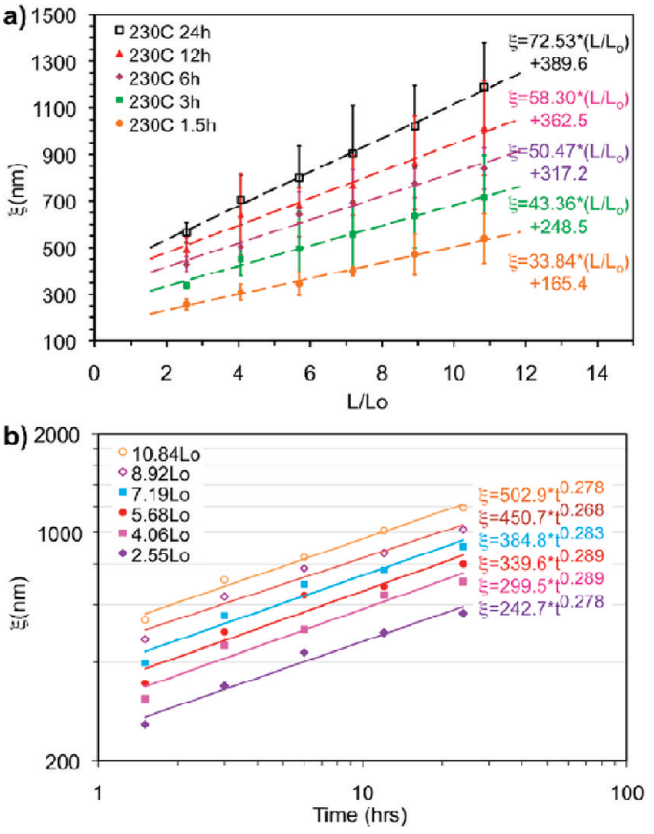

Figure 6. (a) Orientational correlation length (ξ) vs the thickness of C4621 films at different annealing times (1.5−24 h) at 230 °C on 63S-modified substrates. (b) Plot of ξ vs the annealing time (1.5−24 h) at different film thicknesses. The data were reproduced from (a), and the error bars were omitted for clarity. ξ scales with time according to a power law ($\xi \sim t^{\phi}$, $\phi = 0.28 \pm 0.01$).

For example, the thicknesses on top of the islands were $\sim 2L_0$ and $3L_0$ for the films with L of $1.13L_0$ and $2.40L_0$, respectively, and the structures on top of islands were parallel cylinders, similar to the structures on films with thicknesses of $1.98L_0$ and $2.95L_0$ at 230 °C. In the film with $L = 1.58L_0$ that was annealed at 210 °C, islands with parallel cylinders formed with a thickness of $\sim 2L_0$, similar to the structures in films with $L = 1.98L_0$ while perforated structures formed at the lower region. The formation of islands was caused by the incommensurability of L and L_0.[36,52] The perforated structures were due to the complicated interaction between films and the substrate.

The surface morphologies formed in the C4621 films annealed at 190 °C on untreated silicon substrates as well as the films annealed on **63S**-treated silicon substrates can also be understood in terms of the competing effects of the substrate interface and the free surface. In those cases, however, the effect of the free surface and the substrate interface were not as opposed as in the case of the films annealed at 210 and 230 °C on untreated silicon substrates. In the case of the films annealed at 190 °C on untreated silicon substrates, γ for PS and PMMA are slightly different, such that there is not as strong of a driving force to form perpendicular cylinders at the free surface. Indeed, the difference in γ between PS and PMMA at 190 °C may be large enough to result in the formation of defects, such as loops or parallel structures, even on the surface of thicker films. Zhang et al. observed a similar transition from parallel cylinders to mixed parallel and perpendicular cylinders at $\sim 3.7L_0$ using a lower molecular weight PS-*b*-PMMA at 184 °C.[38] In the case of the films annealed on **63S**-treated silicon substrates, the nonpreferential interface created by the **63S** treatment leads to the formation of perpendicular cylinders at the interface. As a result, for the films annealed at 210 and 230 °C, the free surface and interface are both driving the PS-*b*-PMMA to form perpendicular cylinders, usually resulting in the formation of perpendicular cylinders at the free surface at all values of L.

There were two exceptions to the formation of cylinders at the free surface of C4621 films on **63S**-treated silicon substrates, independent of L. First, for the films annealed at 190 °C, the same types of loop or parallel structures appeared when $L > \sim 3L_0$ as were seen in films with $L > \sim 4L_0$ that were annealed on untreated silicon substrates. As was probably the case for the thicker films on untreated silicon substrates, it is likely that the difference in γ between PS and PMMA at 190 °C was large enough to result in the formation of defects.

The second exception is the formation of islands, parallel cylinders, and perforated structures in the films annealed at 230 °C when $L = 1.58L_0$, $1.98L_0$, and $2.40L_0$, respectively. The formation of these structures may have been caused by changes in the interfacial energy of the **63S**-treated substrate with the block copolymer. Just as temperature affects the surface energies of the blocks of a copolymer, it also may affect the interaction between the blocks and the substrate. At a higher temperature, one block may be able to wet the substrate or to penetrate the end-grafted random copolymer brush layer to interact with the underlying silicon substrate. This would effectively change the interfacial energy between each block and the **63S** brush, resulting in the formation of different surface morphologies in films thinner than $3L_0$, as shown in Figure 1b. Within such a range of L, as discussed above, the polymer−substrate interaction determined the domain orientation. For the films annealed at 230 °C, the interaction was apparently sufficiently preferential to drive the formation of parallel domains or island structures. At 210 and 190 °C, the interactions appear to have been sufficiently balanced, such that the substrate was nonpreferential toward either block.[39] In a different approach, instead of changing the annealing temperature, In et al.,[22] Ham et al.,[53] Ji et al.,[16,26] and Han et al.[21] systematically investigated the effect of polymer−substrate interfacial energies on the domain orientation of block copolymer thin films by changing the brush composition. They found that perpendicular orientation of domains was only achieved on brushes with certain composition ranges, on which the interfacial interactions were nearly equal at the specific annealing temperature.

The dynamic study (Figure 3) showed that two independent nucleation events simultaneously occurred at the polymer−substrate and polymer−free surface interfaces. For annealing times less than 10 min, the surface morphologies of the films were only the result of surface nucleation, and the morphology primarily consisted of perpendicular cylinders. After 10 min of annealing, the substrate effect propagated through the film thickness and affected the surface domain orientation. Huge grains of parallel cylinders, for example in the film with L = 95 nm ($3.02L_0$), formed on the surface of the film on untreated silicon substrates due to the strong preferential wetting of PMMA on silicon substrates. The dynamic study also confirmed that the surface morphologies were only determined by the polymer−free surface interaction in thicker films. In the thicker film with L = 340 nm ($10.8L_0$), whether the substrate was untreated silicon or

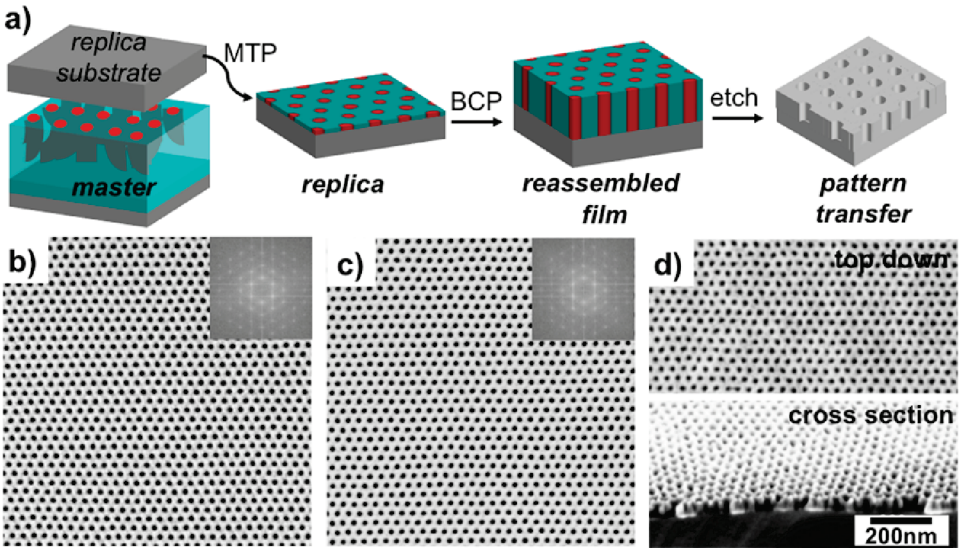

Figure 7. (a) Schematic of MTP from a cylinder-forming ternary blend film and pattern transfer into the underlying silicon oxide substrate by RIE. (b, c) SEM images of a 300 nm thick blend film on a **63S**-modified substrate and a 30 nm thick PS-*b*-PMMA film on the MTP replica after the removal of PMMA blocks by UV exposure and acetic acid washing, respectively. Au (~1 nm) was sputtered on the film surfaces to facilitate SEM imaging in (b) and (c). (d) Top-down and cross-section (45° tilted) SEM images of the silicon oxide pattern after RIE using PS as the etch mask.

63S-treated silicon substrates had no effect on the surface morphology after 10 min of annealing.

Quantification of Grain Sizes on Film Surfaces. We observed that ξ increased linearly with L on both silicon and **63S**-treated silicon substrates (Figure 5). Analogous to Harrison et al.'s observation of sphere-forming block copolymer films,[41] the dominant coarsening process may also be the collapse of small grains into the grain boundaries of larger grains for our cylinder-forming system. The rotation of small grains could be the main pathway to merge with large grains and the possibility of rotating perpendicular cylinders is linearly proportional to the length of cylinders, which may be used to explain the linear correlation between ξ and L. Another plausible explanation could be that the chain mobility at film surfaces depends on the film thickness. In a thin film, an attractive substrate will increase the T_g near the substrate.[54,55] The increase of T_g restricts the polymer chain segmental mobility and results in a reduced diffusion coefficient of polymer chains. Within the film the substrate effect gradually decays, and the chain mobility increases, as the distance from the substrate interface increases. Zheng et al.[56] experimentally observed a similar asymmetric diffusion coefficient profile in thin films on silicon substrates. The diffusion rate at the free surface was faster than that near the substrate interface. As a result, a thicker film should have faster ordering kinetics at film surfaces than a thinner one. In our studies, this effect should lead to a larger ξ in the films with greater L. Within the thickness range that we studied, the decay of the substrate effect may also be proportional to L, which would explain the linear dependence of ξ on L. Although it is experimentally difficult to probe the grain size within a film at different distances from the substrate, it is highly possible that the grain size within the film may be a function of the distance away from the substrate. In analogous work, the grain size of perpendicular lamellae also increased with the film thickness, but scaled with $L^{0.42}$, slower than our cylinder-forming block copolymer system.[57]

There is a slight difference in ξ between C4621 films of equal L annealed on untreated silicon and **63S**-treated silicon substrates, which may be explained by the presence of 2−3 layers of parallel cylinders near the untreated silicon substrates (Figure 2a). The parallel cylinders would reduce the effective thickness of the perpendicular cylinders, as shown in Figure 2a. Considering that ξ is only a function of the thickness of perpendicular cylinders, if we shifted the plot of ξ's on silicon substrates left by $3L_0$, it almost overlapped with the plot of ξ's on **63S**-modified silicon substrates (not shown). Harrison et al. reported similar substrate effect that the ξ of parallel cylinders on PS substrates was larger than that on bare silicon substrates because the brush layer mitigated the substrate pinning.[58]

There was a notable difference in the effect of annealing temperature on ξ, as seen in Figure 5b. While it was not surprising that for films with the same L, an increase of annealing T led to a larger ξ, i.e., $\xi(230\ ^\circ\mathrm{C}) > \xi(210\ ^\circ\mathrm{C}) > \xi(190\ ^\circ\mathrm{C})$, it was interesting that ξ varied linearly with L for annealing at 230 and 210 °C but was constant with L for annealing at 190 °C. It is likely that the lack of variation of ξ with L when annealed at 190 °C was caused by the same phenomena that caused the formation of parallel cylinders or loop defects on film surfaces. We believe both effects were likely caused by a slight difference in the γ of PS and PMMA at 190 °C.

Two aspects of the dependence of ξ on t are worthy of additional discussion. First, the $\xi \sim t^{\phi}$ relationship that we observed, with $\phi = 0.28 \pm 0.01$, was similar to the t dependence for grain sizes observed in thin films containing spherical or cylindrical domains, in which $\phi = 0.25$.[15,30,40−43] We should note that the 0.25 dependence stated in the literature applied to different block copolymers, annealing T, and L. Second, the defect densities decreased quickly within the first 30 min of annealing and did not change noticeably with continued annealing from 1.5 to 24 h in films of equal L. After 1.5 h of annealing, the number of isolated defect pairs decreased during the annealing process; isolated pairs may have fused to form conjugated pairs at the grain boundary. The different behaviors in the first 30 min of annealing and the latter stages of annealing suggest that there may have been different defect annihilation mechanisms occurring during

these two annealing stages. Similarly, Dai et al. also observed two stages of order formation in bulk materials.[44]

The activation energy (E_a) for grain coarsening was roughly estimated assuming that ξ follows the Arrhenius equation, $\xi = A_0 e^{-E_a/RT}$, where A_0 is the coefficient and R is the ideal gas constant. By comparing the ξ's of same thicknesses in Figure 5b annealed at 230 and 210 °C, E_a was roughly estimated to be ~35−43 kJ/mol. E_a of grain coarsening for parallel cylinders of a different block copolymer was estimated to be ~50 kJ/mol, according to the kinetics data reported by Harrison et al.,[15] close to the value of our system.

Replication of Domain Patterns by MTP and Pattern Transfer. The difficulty of using thick PS-*b*-PMMA films as templates for pattern transfer to an underlying substrate may preclude the potential use of the thick PS-*b*-PMMA films. However, MTP provides a method to use the patterns formed on the surface of a thick film to fabricate chemical patterns that can direct the assembly of thin films of block copolymers that could more readily serve as etch masks. The results presented in Figure 7 confirm the efficacy of the MTP technique. A schematic of the MTP process performed with thick films and subsequent pattern transfer into a silicon oxide substrate is shown in Figure 7a.[46] A 300 nm thick ternary blend film was deposited on the **63S**-modified substrate and annealed to form hexagonal arrays of cylinders on the substrate. The ternary blend consists of 90 wt % C4621 and two homopolymer inks, 7 wt % PS-OH and 3 wt % PMMA-OH. The self-assembled cylinders had a ξ of ~1 μm (Figure 7b). During MTP, the homopolymers grafted onto the surface of the replica substrate, reflecting the domain pattern that was on the surface of the self-assembled ternary blend. After MTP and separation, the replica was used to direct the assembly of a 30 nm thick film of the same blend to hexagonal arrays of perpendicular cylinders. ξ of the assembled perpendicular cylinders on the replica was calculated to be ~1 μm, the same as the ξ of the starting thick film (Figure 7c). For the sake of comparison, the ξ of a 30 nm thick PS-*b*-PMMA film that was self-assembled on a neutral brush was only ~200 nm. After directed assembly of the blend film on the MTP replica, the PMMA domains were removed, and the PS matrix was used as an etch mask for pattern transfer into the underlying silicon oxide substrate.[50] Figure 7d shows the top-down and cross-section SEM images of the silicon oxide pattern, indicating the efficient pattern transfer into the 30 nm thick silicon oxide layer. The oxide pattern also had the same ξ as the starting ternary blend template and the MTP replica. The combination of MTP with an initial surface pattern formed in a thick film of block copolymer also demonstrates a route for generating chemical nanopatterns that does not require advanced lithography.

CONCLUSIONS

We demonstrated a facile approach to fabricating hexagonal arrays of perpendicularly oriented cylinders with long-range orientational order by a combined use of high annealing temperatures and large film thicknesses. Our dynamics study proved that independent nucleation events occurred at the polymer−substrate and the polymer−free surface interfaces. We also determined that the surface morphologies were only determined by the polymer−free surface interaction when the film was thicker than a threshold thickness. The technological implication of this approach is that large grain sizes of hexagonal arrays could be easily fabricated without the use of advanced lithographic tools. These patterns could be replicated to make chemical patterns via MTP. The replica patterns in turn could direct the assembly of a thin film of block copolymer for a pattern transfer operation into the underlying substrate, providing a means to fabricate hexagonal arrays of chemical patterns with long-range order for a variety of applications, such as bit patterned media, nanodot memory, and plasmonics.

ASSOCIATED CONTENT

Supporting Information. Figures S1 and S3: SEM images; Figures S2 and S4: the respective Vonoroi plots of Figures S1 and S3. This material is available free of charge via the Internet at http://pubs.acs.org.

AUTHOR INFORMATION

Corresponding Author
*E-mail: nealey@engr.wisc.edu.

ACKNOWLEDGMENT

We thank the funding from UW-NSF Nanoscale Science and Engineering Center (NSEC) (DMR 0832760) and Semiconductor Research Corporation.

REFERENCES

(1) Bates, F. S.; Fredrickson, G. H. *Annu. Rev. Phys. Chem.* **1990**, *41*, 525.
(2) Cheng, J. Y.; Ross, C. A.; Thomas, E. L.; Smith, H. I.; Vancso, G. J. *Adv. Mater.* **2003**, *15*, 1599.
(3) Daoulas, K. C.; Muller, M.; Stoykovich, M. P.; Park, S. M.; Papakonstantopoulos, Y. J.; de Pablo, J. J.; Nealey, P. F.; Solak, H. H. *Phys. Rev. Lett.* **2006**, 96.
(4) Kang, H.; Craig, G. S. W.; Nealey, P. F. *J. Vac. Sci. Technol., B* **2008**, *26*, 2495.
(5) Park, M.; Harrison, C.; Chaikin, P. M.; Register, R. A.; Adamson, D. H. *Science* **1997**, *276*, 1401.
(6) Segalman, R. A.; Yokoyama, H.; Kramer, E. J. *Adv. Mater.* **2001**, *13*, 1152.
(7) Stein, G. E.; Kramer, E. J.; Li, X.; Wang, J. *Phys. Rev. Lett.* **2007**, 98.
(8) Stein, G. E.; Kramer, E. J.; Li, X. F.; Wang, J. *Macromolecules* **2007**, *40*, 2453.
(9) Kim, S. O.; Solak, H. H.; Stoykovich, M. P.; Ferrier, N. J.; de Pablo, J. J.; Nealey, P. F. *Nature* **2003**, *424*, 411.
(10) Park, S. M.; Craig, G. S. W.; La, Y. H.; Nealey, P. F. *Macromolecules* **2008**, *41*, 9124.
(11) Park, S. M.; Craig, G. S. W.; La, Y. H.; Solak, H. H.; Nealey, P. F. *Macromolecules* **2007**, *40*, 5084.
(12) Stoykovich, M. P.; Kang, H.; Daoulas, K. C.; Liu, G.; Liu, C. C.; de Pablo, J. J.; Mueller, M.; Nealey, P. F. *ACS Nano* **2007**, *1*, 168.
(13) Stoykovich, M. P.; Muller, M.; Kim, S. O.; Solak, H. H.; Edwards, E. W.; de Pablo, J. J.; Nealey, P. F. *Science* **2005**, *308*, 1442.
(14) Knoll, A.; Horvat, A.; Lyakhova, K. S.; Krausch, G.; Sevink, G. J. A.; Zvelindovsky, A. V.; Magerle, R. *Phys. Rev. Lett.* **2002**, *89*, 035501.
(15) Harrison, C.; Adamson, D. H.; Cheng, Z. D.; Sebastian, J. M.; Sethuraman, S.; Huse, D. A.; Register, R. A.; Chaikin, P. M. *Science* **2000**, *290*, 1558.
(16) Ji, S. X.; Liu, G. L.; Zheng, F.; Craig, G. S. W.; Himpsel, F. J.; Nealey, P. F. *Adv. Mater.* **2008**, *20*, 3054.
(17) Xu, T.; Hawker, C. J.; Russell, T. P. *Macromolecules* **2005**, *38*, 2802.

(18) Peters, R. D.; Yang, X. M.; Kim, T. K.; Nealey, P. F. *Langmuir* **2000**, *16*, 9620.
(19) Peters, R. D.; Yang, X. M.; Kim, T. K.; Sohn, B. H.; Nealey, P. F. *Langmuir* **2000**, *16*, 4625.
(20) Peters, R. D.; Yang, X. M.; Wang, Q.; de Pablo, J. J.; Nealey, P. F. *J. Vac. Sci. Technol., B* **2000**, *18*, 3530.
(21) Han, E.; Stuen, K. O.; La, Y. H.; Nealey, P. F.; Gopalan, P. *Macromolecules* **2008**, *41*, 9090.
(22) In, I.; La, Y. H.; Park, S. M.; Nealey, P. F.; Gopalan, P. *Langmuir* **2006**, *22*, 7855.
(23) Mansky, P.; Liu, Y.; Huang, E.; Russell, T. P.; Hawker, C. J. *Science* **1997**, *275*, 1458.
(24) Ryu, D. Y.; Shin, K.; Drockenmuller, E.; Hawker, C. J.; Russell, T. P. *Science* **2005**, *308*, 236.
(25) Ryu, D. Y.; Wang, J. Y.; Lavery, K. A.; Drockenmuller, E.; Satija, S. K.; Hawker, C. J.; Russell, T. P. *Macromolecules* **2007**, *40*, 4296.
(26) Ji, S. X.; Liao, W.; Nealey, P. F. *Macromolecules* **2010**, *43*, 6919.
(27) Park, S. M.; Craig, G. S. W.; Liu, C. C.; La, Y. H.; Ferrier, N. J.; Nealey, P. F. *Macromolecules* **2008**, *41*, 9118.
(28) Cheng, J. Y.; Rettner, C. T.; Sanders, D. P.; Kim, H. C.; Hinsberg, W. D. *Adv. Mater.* **2008**, *20*, 3155.
(29) Park, S. M.; Stoykovich, M. P.; Ruiz, R.; Zhang, Y.; Black, C. T.; Nealey, P. E. *Adv. Mater.* **2007**, *19*, 607.
(30) Ruiz, R.; Sandstrom, R. L.; Black, C. T. *Adv. Mater.* **2007**, *19*, 587.
(31) Ruiz, R.; Kang, H. M.; Detcheverry, F. A.; Dobisz, E.; Kercher, D. S.; Albrecht, T. R.; de Pablo, J. J.; Nealey, P. F. *Science* **2008**, *321*, 936.
(32) Han, E.; Stuen, K. O.; Leolukman, M.; Liu, C. C.; Nealey, P. F.; Gopalan, P. *Macromolecules* **2009**, *42*, 4896.
(33) Chuang, V. P.; Ross, C. A.; Gwyther, J.; Manners, I. *Adv. Mater.* **2009**, *21*, 3789.
(34) Ji, S.; Liu, C. C.; Son, J. G.; Gotrik, K.; Craig, G. S. W.; Gopalan, P.; Himpsel, F. J.; Char, K.; Nealey, P. F. *Macromolecules* **2008**, *41*, 9098.
(35) Jung, Y. S.; Jung, W.; Ross, C. A. *Nano Lett.* **2008**, *8*, 2975.
(36) Mansky, P.; Russell, T. P.; Hawker, C. J.; Pitsikalis, M.; Mays, J. *Macromolecules* **1997**, *30*, 6810.
(37) Wu, S. *J. Phys. Chem.* **1970**, *74*, 632.
(38) Zhang, X. H.; Berry, B. C.; Yager, K. G.; Kim, S.; Jones, R. L.; Satija, S.; Pickel, D. L.; Douglas, J. F.; Karim, A. *ACS Nano* **2008**, *2*, 2331.
(39) Suh, H. S.; Kang, H.; Nealey, P. F.; Char, K. *Macromolecules* **2010**, *43*, 4744.
(40) Black, C. T.; Guarini, K. W. *J. Polym. Sci., Part A: Polym. Chem.* **2004**, *42*, 1970.
(41) Harrison, C.; Angelescu, D. E.; Trawick, M.; Cheng, Z. D.; Huse, D. A.; Chaikin, P. M.; Vega, D. A.; Sebastian, J. M.; Register, R. A.; Adamson, D. H. *Europhys. Lett.* **2004**, *67*, 800.
(42) Harrison, C.; Cheng, Z. D.; Sethuraman, S.; Huse, D. A.; Chaikin, P. M.; Vega, D. A.; Sebastian, J. M.; Register, R. A.; Adamson, D. H. *Phys. Rev. E* **2002**, *66*, 011706.
(43) Vega, D. A.; Harrison, C. K.; Angelescu, D. E.; Trawick, M. L.; Huse, D. A.; Chaikin, P. M.; Register, R. A. *Phys. Rev. E* **2005**, *71*, 061803.
(44) Dai, H. J.; Balsara, N. P.; Garetz, B. A.; Newstein, M. C. *Phys. Rev. Lett.* **1996**, *77*, 3677.
(45) Kim, S. H.; Misner, M. J.; Xu, T.; Kimura, M.; Russell, T. P. *Adv. Mater.* **2004**, *16*, 226.
(46) Ji, S. X.; Liu, C. C.; Liu, G. L.; Nealey, P. F. *ACS Nano* **2010**, *4*, 599.
(47) Benoit, D.; Chaplinski, V.; Braslau, R.; Hawker, C. J. *J. Am. Chem. Soc.* **1999**, *121*, 3904.
(48) Liu, C. C.; Craig, G. S. W.; Kang, H. M.; Ruiz, R.; Nealey, P. F.; Ferrier, N. J. *J. Polym. Sci., Polym. Phys.* **2010**, *48*, 2589.
(49) Ostu, N. *IEEE Trans. Syst. Man Cybernet* **1979**, *9*, 62.
(50) Liu, C. C.; Nealey, P. F.; Ting, Y. H.; Wendt, A. E. *J. Vac. Sci. Technol., B* **2007**, *25*, 1963.
(51) Welander, A. M.; Kang, H. M.; Stuen, K. O.; Solak, H. H.; Muller, M.; de Pablo, J. J.; Nealey, P. F. *Macromolecules* **2008**, *41*, 2759.
(52) Coulon, G.; Collin, B.; Ausserre, D.; Chatenay, D.; Russell, T. P. *J. Phys. (Paris)* **1990**, *51*, 2801.
(53) Ham, S.; Shin, C.; Kim, E.; Ryu, D. Y.; Jeong, U.; Russell, T. P.; Hawker, C. J. *Macromolecules* **2008**, *41*, 6431.
(54) Akabori, K.; Tanaka, K.; Nagamura, T.; Takahara, A.; Kajiyama, T. *Macromolecules* **2005**, *38*, 9735.
(55) Torres, J. A.; Nealey, P. F.; de Pablo, J. J. *Phys. Rev. Lett.* **2000**, *85*, 3221.
(56) Zheng, X.; Rafailovich, M. H.; Sokolov, J.; Strzhemechny, Y.; Schwarz, S. A.; Sauer, B. B.; Rubinstein, M. *Phys. Rev. Lett.* **1997**, *79*, 241.
(57) Sivaniah, E.; Hayashi, Y.; Matsubara, S.; Kiyono, S.; Hashimoto, T.; Kukunaga, K.; Kramer, E. J.; Mates, T. *Macromolecules* **2005**, *38*, 1837.
(58) Harrison, C.; Chaikin, P. M.; Huse, D. A.; Register, R. A.; Adamson, D. H.; Daniel, A.; Huang, E.; Mansky, P.; Russell, T. P.; Hawker, C. J.; Egolf, D. A.; Melnikov, I. V.; Bodenschatz, E. *Macromolecules* **2000**, *33*, 857.

NOTE ADDED AFTER ASAP PUBLICATION

This article posted ASAP on April 29, 2011. Figure 1 has been revised. The correct version posted on May 4, 2011.